MULTIFRAGMENTATION IN PERIPHERAL NUCLEUS-NUCLEUS COLLISIONS*

W. TRAUTMANN,[a] J.C. ADLOFF,[c] M. BEGEMANN-BLAICH,[a]
P. BOUISSOU,[d] J. HUBELE,[a] G. IMME,[e] I. IORI,[f] P. KREUTZ,[b]
G.J. KUNDE,[a] S. LERAY,[d] V. LINDENSTRUTH,[a] Z. LIU,[a] U. LYNEN,[a]
R.J. MEIER,[a] U. MILKAU,[a] A. MORONI,[f] W.F.J. MÜLLER,[a] C. NGÔ,[d]
C.A. OGILVIE,[a] J. POCHODZALLA,[a] G. RACITI,[e] G. RUDOLF,[c]
H. SANN,[a] A. SCHÜTTAUF,[b] W. SEIDEL,[g] L. STUTTGE,[c]
AND A. TUCHOLSKI[a]

[a] Gesellschaft für Schwerionenforschung, D-64220 Darmstadt, Germany
[b] Institut für Kernphysik, Universität Frankfurt, D-60486 Frankfurt, Germany
[c] Centre de Recherches Nucléaires, F-67037 Strasbourg, France
[d] Laboratoire National Saturne, CEN Saclay, F-91191 Gif-sur-Yvette, France
[e] Dipartimento di Fisica dell' Universitá and I.N.F.N., I-95129 Catania, Italy
[f] Istituto di Scienze Fisiche, Universitá degli Studi di Milano and I.N.F.N. I-20133 Milano, Italy
[g] Forschungszentrum Rossendorf, Postfach 510119, D-01314 Dresden, Germany

(Received October 26, 1993)

The complete fragmentation of highly excited nuclear systems into fragments of intermediate mass is observed in heavy-ion reactions at relativistic bombarding energies in the range of several hundreds of MeV per nucleon. Similar features are found for peripheral collisions between heavy nuclei and for more central collisions between a heavy and a light nucleus. The partition space explored in multifragment decays is well described by the statistical multifragmentation models. The expansion before breakup is confirmed by the analysis of the measured fragment energies of ternary events in their own rest frame. Collective radial flow is confined to rather small values in these peripheral-type reactions. Many conceptually different models seem to be capable of reproducing the charge correlations measured for the multifragment decays.

PACS numbers: 25.40. Sc, 25.70. Gh, 25.70. Mn, 25.70. Pq

---

* Presented at the XXIII Mazurian Lakes Summer School on Nuclear Physics, Piaski, Poland, August 18–28, 1993.

1. Introduction

The statistical multifragmentation models consider the phase space available for excited and expanded nuclear systems which are in equilibrium and have the possibility to partition into any number of particles and nuclear fragments [1, 2]. The input parameters to these models are the excitation energy E_x and the mass of A_0 nucleons that form the system. The ways of choosing the volume of about 4 to 6 times the normal nuclear volume are properties of the models. A comparison of the Berlin and Copenhagen versions has very recently been presented by Gross and Sneppen [3].

As a function of the excitation energy the statistical weights for the multi-fragment configurations assume a maximum near $E_x = 8$ MeV per nucleon. Multi-fragment emission was predicted to be the dominant decay mode at these energies close to the limit of nuclear binding [4]. At lower energies the required surface energy for fragment formation is not easily available, and most of the nucleons are found forming a large residue. Above 8 MeV per nucleon the system needs all the available degrees of freedom in order to accommodate the higher energies. There it approaches the complete disassembly into nucleons and light complex particles.

These predictions carry a high significance in several respects: First, multifragmentation constitutes a new decay mechanism for highly excited nuclear matter with new properties, different from the known mechanisms of evaporation and fission. Second, the fragmentation of a system into several parts of varying sizes is a phenomenon encountered in many other fields of physics. Critical phenomena may be expected [5]. And third, the breakup may occur at densities corresponding to the mechanically unstable spinodal region of nuclear matter and thus provide information on the predicted liquid-gas phase transition of nuclear matter [6]. Great efforts were therefore made in order to answer the experimental questions: Can we produce such excited and expanded systems and will they fragment as predicted?

It was suggested that the compression-expansion cycle expected for heavy-ion reactions at high energies may lead into the unstable region [7]. The corresponding reaction trajectory is labelled "central" in Fig. 1 where it is assumed that the expansion proceeds isentropically. Recent results from the study of central collisions of very heavy nuclei are presented in the contribution of the FOPI collaboration to this volume [8]. Abundant production of intermediate-mass fragments was also observed in reactions induced by protons or light complex projectiles with energies in the GeV range. The multiplicities of selected events were found to be large [9, 10]. A significant compression is not expected in these reactions. On the contrary, the density may even decrease during the excitation phase when spectator nucleons are knocked out by cascading hadrons. A subsequent expansion may be driven by the build-up of thermal pressure [11].

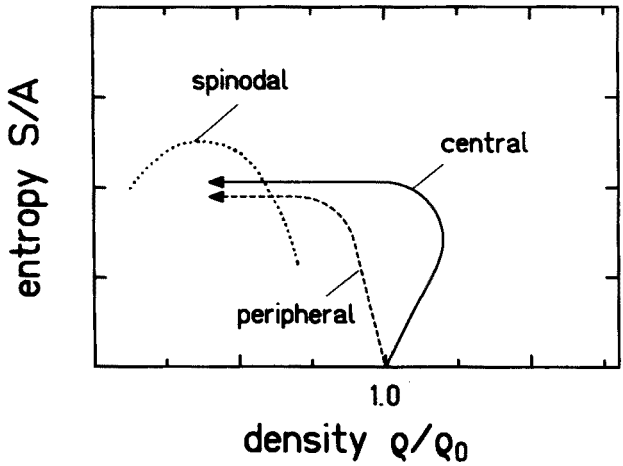

Fig. 1. Schematic illustration of the reaction paths for central and peripheral heavy-ion reactions in the entropy versus density plane.

The same kind of mechanism is also expected for peripheral collisions of heavy nuclei at relativistic energies (trajectory labelled "peripheral" in Fig. 1). The fireball formed by the participants in the overlap zone represents an intense source of fast particles which may heat and deplete the spectator matter. The abrasion of the fireball nucleons from the collision partners is an additional source of excitation [12]. In the following, we will be concerned with this type of reaction and with its capabilities to produce fragmenting spectator systems. The presented data were obtained by the ALADIN collaboration in recent experiments with beams from the SIS facility.

2. Reaction studies in inverse kinematics

Multifragment events have been observed in emulsion studies when the first heavy-ion beams with relativistic energies became available [13]. It was noticed early on that reactions of a peripheral type may lead to rather violent disintegration processes [14]. The decay of heavy projectiles was also studied with plastic nuclear-track detectors which provide high Z-resolution above a threshold near $Z = 6$ [15]. A recent analysis of emulsion data for ^{84}Kr interactions at $E/A = 1.52$ GeV was presented in Ref. [16].

The ALADIN forward-spectrometer at GSI is designed for the study of the projectile decay in inverse kinematics. A schematic layout of the experimental setup, used during the first experiments with beams of ^{197}Au at a bombarding energy of $E/A = 600$ MeV, is shown in Fig. 2.

For each projectile nucleus, its position and arrival time were measured upstream of the target with two thin plastic scintillators. Targets of C, Al,

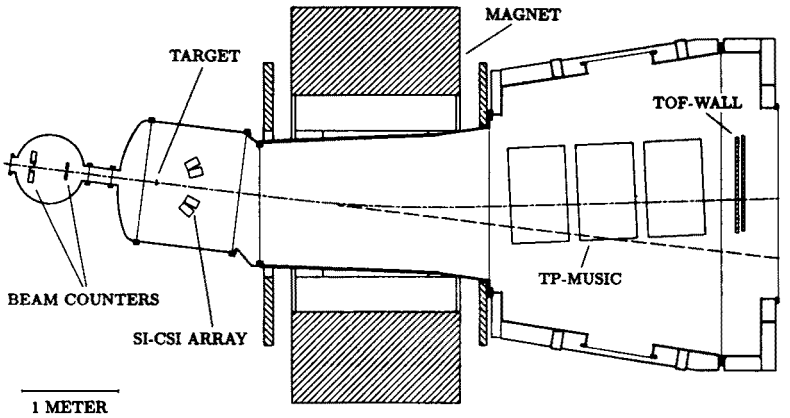

Fig. 2. Cross-sectional view of the ALADIN facility. The beam enters from the left and is monitored by the beam counters before reaching the target. Mid-rapidity particles are detected in the Si-CsI array. Projectile fragments are tracked and identified in the TP-MUSIC and in the time-of-flight wall. The dashed line indicates the direction of the incident beam. The dash-dotted line represents the trajectory of beam particles after they were deflected by an angle of 8.2° (from [17]).

Cu, and Pb with areal densities between 200 and 700 mg/cm^2 were used. The acceptance of the ALADIN spectrometer for beam velocity fragments with $N = Z$ was $\pm$ 4.7° in the horizontal and $\pm$ 4.5° in the vertical direction. This range proved to be sufficient to detect virtually all of the fragments originating from the decay of the gold projectiles.

The atomic numbers Z and the multiplicity of nuclear fragments were determined by means of the time-of-flight (TOF) wall which was positioned at a distance from the target of approximately 6 m. The wall consisted of two layers, with 40 vertical scintillators each, and covered an area of 1 m $\times$ 1.1 m. Individual elements were resolved for $Z \leq 10$, and a charge resolution of $\pm$ 2 for heavier fragments was obtained. Fragments with $Z \geq 8$ were identified with individual Z resolution by the multiple-sampling ionization chamber (TP-MUSIC).

Light particles, predominantly originating from the mid-rapidity source, were detected by the 64 elements of a Si-CsI(Tl) hodoscope, placed near the target at angles between 7° and 40°. The detection of at least one particle by the hodoscope was a software condition applied throughout the analysis of the data.

The magnetic rigidity of detected projectile fragments was determined by measuring their trajectories with the TP-MUSIC detector located between the magnet and the TOF-wall (Fig. 2). The track positions along the flight path through the detector were derived from the drift times of the ionization charges measured consecutively in the perpendicular x-, y-,

and again x-directions in the three field cages. The point of interaction in the target, in the plane perpendicular to the beam direction, was determined with a position-sensitive plastic detector upstream of the target. The emission angle and the rigidity R were then obtained by fitting with a set of calculated trajectories. For the primary gold projectiles a rigidity resolution of $\Delta R/R = 1.2\%$ was achieved.

The momenta P were derived from $P = Q \cdot R$. Since basically all fragments of interest are fully stripped Q is equal to Z and can be determined with the TP-MUSIC detector. The obtained resolution was $\Delta Z = \Delta Q = 0.5$ charge units (FWHM). Masses were determined from $P = M\gamma\beta c$, where the velocity $v = \beta c$ and γ were derived from the measured time of flight and from the length of the tracked flight path. The mass resolution $\Delta M/M = \gamma^2 \Delta t/t + \Delta P/P$ was limited by the time resolution $\Delta t/t \approx 1\%$ because $\gamma^2 = 2.6$ at $E/A = 600$ MeV. With the resulting resolution of the order of 3% individual masses of the lighter fragments were resolved.

3. Impact parameter and Z_{bound}

The quantity Z_{bound} was found very useful for the ordering of the observed fragmentation events [17]. Z_{bound} is defined as the sum of the atomic numbers of all fragments and complex particles with $Z \geq 2$ that are detected with the TOF wall. Z_{bound} is a good approximation to the atomic number of the decaying spectator system. Reaction products with approximately projectile velocity are selected by the acceptance of the spectrometer and detected without threshold (Fig. 3). Only the hydrogen isotopes from the decay of the projectile spectator and from the subsequent decay of excited fragments are not included in Z_{bound}.

Because of the geometric properties of the reaction mechanism at relativistic energies the participant zone increases with decreasing impact parameter [18]. The remaining projectile spectator, and thus Z_{bound}, decreases. This correlation of Z_{bound} with the impact parameter is supported by simulations with the BUU model [19]. At the same time, Z_{bound} is also correlated with the excitation energy of the spectator system. The amount of extra surface created by abrasion and the intensity of the fireball which acts as a heat source increase with decreasing impact parameter and thus with decreasing Z_{bound}. In the experiment, the intensity of the fireball is measured by the number M_{lp} of light charged particles detected at midrapidity with the Si-CsI hodoscope.

The measured yields of intermediate-mass fragments as functions of M_{lp} and of Z_{bound} are shown in Fig. 4. Intermediate-mass fragments (IMF's) are here defined as reaction products with atomic numbers in the range $3 \leq Z \leq 30$. The two sets of distributions are basically identical. In either

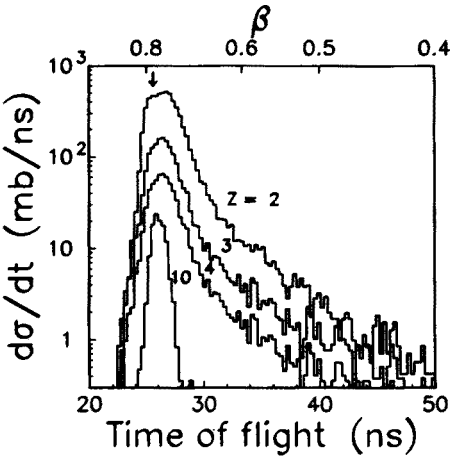

Fig. 3. Time-of-flight spectra of fragments with $Z = 2, 3, 4, 10$ produced in Au + Cu reactions. The top scale gives the approximate velocity of the fragments, calculated from the time of flight by assuming a fixed path length for all particles. For fragments with $Z > 10$ this is correct within 0.5%. The arrow indicates the beam velocity (from [17]).

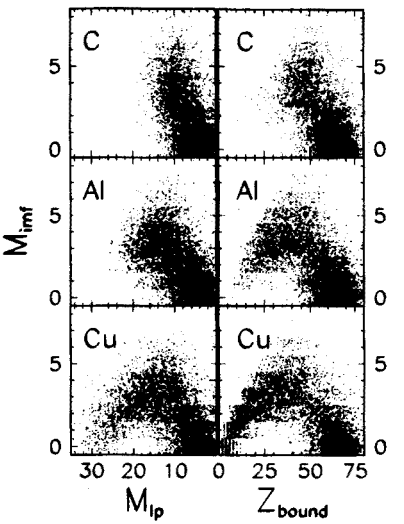

Fig. 4. Multiplicity of intermediate-mass fragments as a function of the multiplicity M_{lp} of light particles detected in the Si-CsI array (left panel) and as a function of Z_{bound} (right panel). Note that M_{lp} runs from right to left. Random numbers, taken from the interval [-0.5,0.5], were added to the integer values M_{imf} in order to preserve the intensity information in the scatter plot.

case the impact parameter decreases from the right to the left. We observe that in the reactions with the carbon target the multiplicity of fragments increases with decreasing impact parameter and reaches its maximum at the most central collisions. In the reactions with the heavier targets a maximum is reached at mid-central collisions. Then, towards the most central collisions, the fragment multiplicity decreases again. This was termed the rise and fall of multi-fragment decay [20].

It is important to keep in mind that both, the excitation energy and the mass of the decaying system, vary with Z_{bound}. This has to be taken into account if comparisons to model calculations are made.

4. The rise and fall of multifragment production

The mean values of the multiplicity distributions of intermediate-mass fragments are shown in Fig. 5. The rise and fall with decreasing Z_{bound} and thus with decreasing impact parameter is clearly observed in the reactions with the heavier targets. For a given Z_{bound} the mean fragment multiplicity is independent of the target. This feature, called Z_{bound}-scaling, was found to be a rather general phenomenon. The widths, charge asymmetries, and other charge correlations describing the partition into fragments are target independent if plotted as functions of Z_{bound} [21].

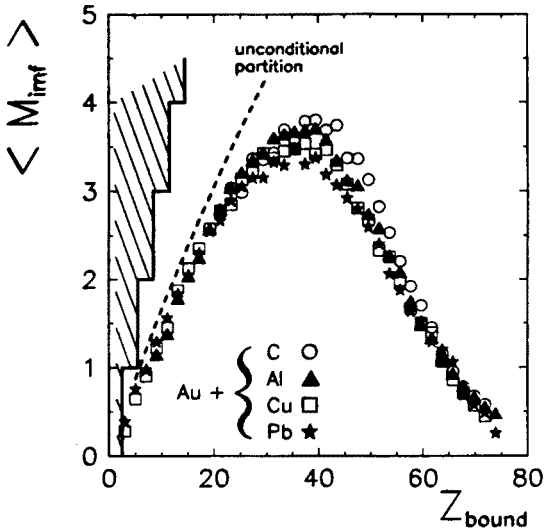

Fig. 5. Correlation between the mean multiplicity of intermediate-mass fragments $\langle M_{\mathrm{imf}} \rangle$ and Z_{bound} for the reactions of Au with C, Al, Cu, and Pb targets at $E/A = 600$ MeV. The hatched area is excluded because of the lower limit $Z = 3$ for intermediate-mass fragments. The dashed line is the result of an unconditional Z partition of finite systems with $Z < 40$ (from [24]).

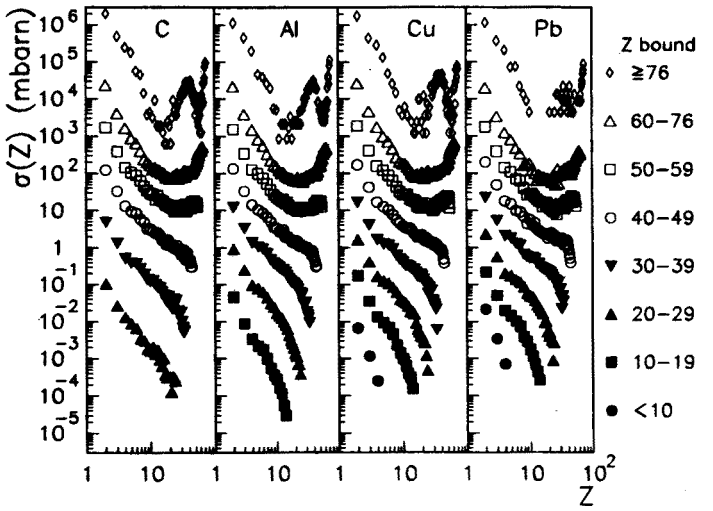

Fig. 6. Measured Z distributions of fragments with atomic number $Z \geq 2$ for the reactions of Au with C, Al, Cu, and Pb targets at $E/A = 600$ MeV and for distinct intervals of Z_{bound} as indicated on the right. For each target the data have been multiplied by the following factors, in decreasing order of Z_{bound}: 10^4, 10^2, 1, 10^{-1}, 10^{-2}, 10^{-3}, 10^{-4}, and 10^{-5}. The error bars are in most cases smaller than the size of the symbols (from [21]).

Differentiating between the rise, the maximum, and the fall of the fragment multiplicities, we may discuss these three regions by looking at the Z_{bound}-gated element spectra (Fig. 6). At large Z_{bound} we find U-shaped spectra with a minimum near $Z = 20$. Such spectra are familiar from heavy-ion reactions at intermediate bombarding energies and from light-particle induced reactions. The produced spectator nuclei decay by emitting up to a few fragments among many light particles, and a heavy residue remains. In the region of the maximum fragment multiplicity near $Z_{\mathrm{bound}} \approx 40$ the rise towards large Z has disappeared. The element distributions have assumed a power-law shape. We observe the complete fragmentation of the excited spectator system. The scatter plots (Fig. 4) show that here the widths of the multiplicity distributions are smaller than the mean values. Fragmentation into several fragments is the dominant decay mode observed. In the fall region at very small Z_{bound} the element spectra drop more rapidly, partly due to the autocorrelations caused by the cut on Z_{bound}. There the mean number of fragments follows closely the expectation for an unconditional partition of the decaying system [22, 23].

5. Statistical descriptions

The analysis of these data in the framework of the statistical multifragmentation models has recently made a remarkable progress. First it was shown that statistical models that include an expansion of the excited nuclear system can account for the observed fragment multiplicities while sequential models, assuming successive binary decays at normal nuclear density, yield fragment multiplicities which are too small [24]. In these calculations the input to the statistical models, *i.e.* the size and excitation energy of the decaying systems, was provided by calculations with the BUU model. They were performed and analyzed in order to describe the primary stage of the reaction. Soon after, several groups were able to show that not only the multiplicities of intermediate-mass fragments but also the measured asymmetries and higher-order charge correlations [21] can be reproduced to high accuracy with the statistical multifragmentation models [25–27]. This was achieved by rather freely varying the initial mass or excitation energy or both. It turns out, in particular for the more central collisions, that the so determined equilibrated energy is significantly smaller than the energy deposited in the system according to the BUU model (Fig. 7). The excitation energy per nucleon resulting from these analyses consistently saturates at values $E_x/A \approx 6$ to 8 MeV.

At present, these results permit two conclusions to be drawn: In the rise and in the maximum regions of the fragment multiplicities, the excitation energies derived from treating the initial stage with the BUU model and by treating the exit-channel configurations with the statistical multifragmentation model agree, at least qualitatively. The statistical models give a good description of the phase space for multi-fragment decays as it opens with increasing excitation energy. This also holds for the sequential statistical model of Friedman which allows for expansion of the system under thermal pressure [24, 28]. Secondly, also including the fall region, the statistical models give a good description of the partition space, *i.e.* of the distributions and correlations of the element numbers. This, however, is not unique for these models. The fragment multiplicities and charge correlations were also well reproduced with other models, including site-bond-percolation [21], classical-cluster formation [29], fragmentation-inactivation binary [30], and restructured-aggregation models [31]. The underlying symmetries, apparently common to all of these models, remain to be revealed. Some of the models are of a purely mathematical nature, have very few parameters, and do not contain any of the nuclear physics input on which the statistical models are based. Some exhibit critical behaviour in the limit of an infinite number of constituents.

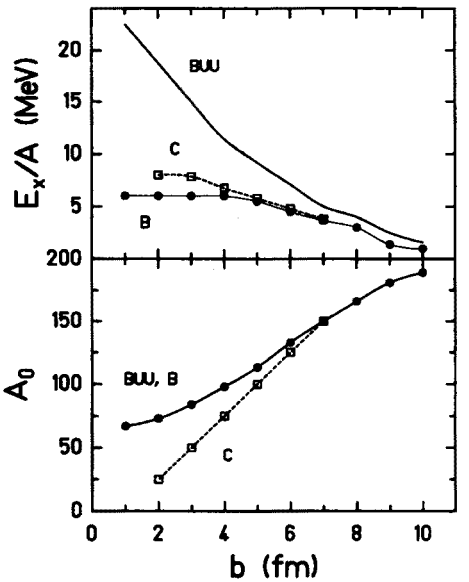

Fig. 7. Excitation energy per nucleon (top) and mass of the system (bottom) as calculated with the BUU model in Ref. [21] and as derived from the analyses with the Berlin (B, Ref. [26]) and Copenhagen (C, Ref. [27]) statistical multifragmentation models.

6. Dynamical observables

The apparent success of the statistical models represents a challenge for dynamical analyses based on measured fragment energies and momenta. Predictions may be obtained by using the breakup configurations provided by the statistical models and by following the trajectories of reaction products until they reach the detectors. This requires a realistic treatment of the mutual Coulomb repulsions and of the subsequent decay of excited fragments.

In the following, we present first results from the tracking analysis of the fragmentation data taken with the ALADIN spectrometer [32]. It was performed for the subset of events in which three fragments are above the tracking threshold $Z \geq 8$ of the TP-MUSIC detector. Due to this constraint, this event sample extends over the range $Z_{\mathrm{bound}} \approx 40$ to 70, *i.e.* it covers part of the maximum and the rise part of the multiplicity distributions (Fig. 5). In the first step of the analysis, the velocities of the three tracked fragments were transformed into their common center-of-mass system. From the resulting velocities v_i and the measured masses m_i the sum of the kinetic

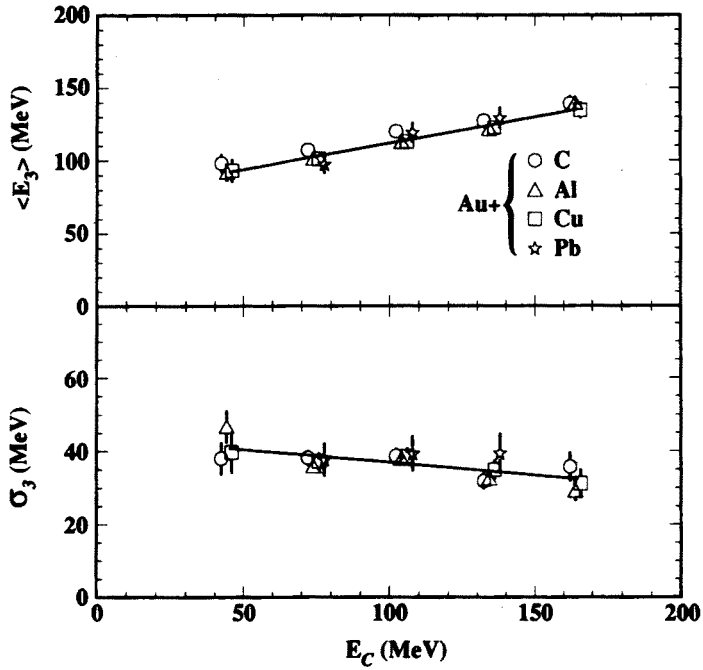

Fig. 8. Mean center-of-mass total kinetic energy $\langle E_3 \rangle$ (top) and the standard deviation σ_3 (bottom) as a function of the nominal Coulomb energy E_C for the three largest projectile fragments emitted in Au + C, Al, Cu and Pb collisions at $E/A = 600$ MeV. The points were obtained by sorting the data in 30 MeV wide bins (from [32]).

energies in the center-of-mass system

$$E_3 = \sum_{i=1}^{3} m_i \frac{v_i^2}{2}, \tag{1}$$

was calculated. The mean value and the width of this quantity is plotted in Fig. 8 as a function of the sum of the mutual Coulomb energies

$$E_C = e^2 \sum_{i<j} \frac{Z_i Z_j}{r_0 \left(A_i^{1/3} + A_j^{1/3} \right)}. \tag{2}$$

For the radius parameter r_0 a value of 1.4 fm was used. E_C, in first place, is to be taken as a parameterization of the charge composition of the ternary events rather than the sum of the actual mutual repulsions. The mean value $\langle E_3 \rangle$ rises as a function of E_C but not directly in proportion to it. This shows that other sources contribute to the kinetic energies, such as *e.g.* thermal motion.

A second type of observable deduced from the measured velocities is the fragment-fragment correlation function. It is expected to be sensitive to the time scale of the breakup process [33]. The mutual interaction between two fragments emitted from a third one depends on their relative separation in space and thus also on the time interval between the two emissions. Therefore, for the studied class of ternary events, the correlation function was constructed from the relative velocities

$$v_{\mathrm{rel}} = |\vec{v}_2 - \vec{v}_3|\,, \tag{3}$$

of the two lighter fragments of each event. It is shown in Fig. 9 as a function of the reduced velocity

$$\beta_{\mathrm{red}} = \frac{\frac{v_{\mathrm{rel}}}{c}}{\sqrt{Z_2 + Z_3}} \tag{4}$$

which contains a first order correction for the effect of the two fragment charges on their relative velocity [34]. Events with different pairs Z_2 and Z_3 may thus be plotted together in the same figure. The measured coincidence yield is shown in the bottom part of Fig. 9. The knowledge of the mass and velocity of the largest fragment is important in this analysis because it enters into the calculation of the uncorrelated yields in the following way: the uncorrelated yields are obtained from the same event sample by choosing fragments from different events under otherwise identical conditions (event mixing). Their relative velocities depend on the center-of-mass velocities of the two three-body-systems which, in turn, depend predominantly on the mass and velocity of the heaviest fragment.

The data of Figs 8 and 9 represent a test for any model aiming at a description of the temporal and spatial breakup configurations. The curves shown in Fig. 9 are the results of three-body Coulomb calculations performed for a sequential breakup scenario [32]. In addition to the initial spatial and temporal separations of the fragments also the thermal velocity components and the effects of particle evaporation from the separated fragments are considered. It is found that the choice of parameters is strongly restricted by the experimental data. The widths σ_3 require initial temperatures of $f_T \approx 1.25$ times the values obtained from the BUU calculations for the primary stage of the reaction. The Coulomb contributions to E_3 are thereby restricted which requires large initial separations between the surfaces of the two fragments, $2D \approx 4$ fm. With these parameters being fixed, the correlation functions were found to be sensitive to the time intervals between the emissions (Fig. 9). The best approximation to the data was obtained with the rather short time scale of $\tau = 10$ fm/c.

The sequential breakup scenario with the obtained parameters is equivalent to a simultaneous breakup of an excited and expanded system. The

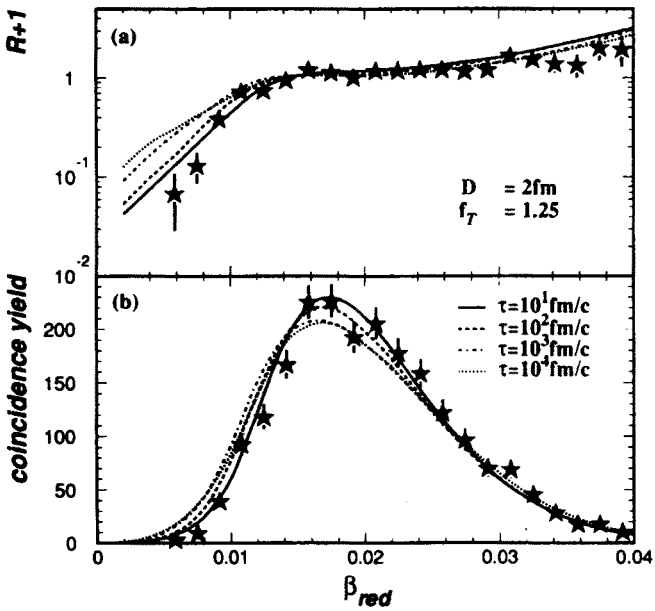

Fig. 9. Correlation function (top) and coincidence yield (bottom) as a function of the reduced velocity β_{red}. The data points represent the total statistics from the reactions on all four targets. The input parameters to the model calculations are indicated (from [32]).

analysis qualitatively confirms the results of the statistical analysis for the region of Z_{bound} near the maximum of the fragment multiplicity. The same data were also reproduced with trajectory calculations based on a simultaneous breakup scenario that included the possibility of collective radial flow. It was found that the contribution from flow to the observed fragment energies is limited to about 1 MeV per nucleon but more likely close to zero [32]. This is contrary to the large radial flow reported for a selected class of central collisions in Au + Au collisions [8].

7. Present systematics

The fragment multiplicities and the excitation energies E_x residing in the decaying system have been measured by Trockel *et al.* for a set of reactions in the intermediate range of bombarding energies near the onset of multifragment production [35]. A maximum of 0.5 fragments associated with central collisions of ^{40}Ar + ^{197}Au at $E/A = 30$ MeV was observed in this study. The excitation energy deduced for this case was about 4 MeV per nucleon. Larger fragment multiplicities with mean values of more than four were found by de Souza *et al.* for the reaction ^{36}Ar + ^{197}Au when

the bombarding energy was raised up to 110 MeV per nucleon [36]. Even larger multiplicities were observed in reactions with larger projectiles such as ^{129}Xe at E/A = 50 MeV [37] or ^{208}Pb at E/A = 29 MeV [38], all on gold targets.

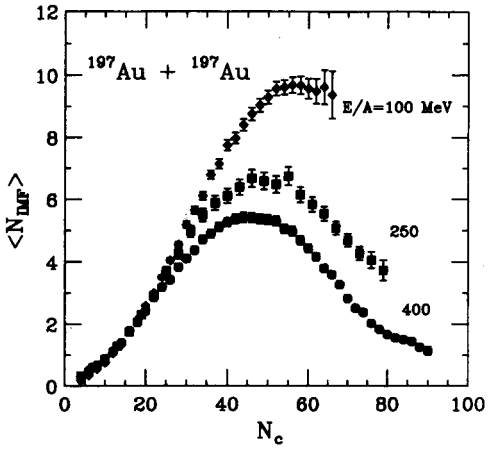

Fig. 10. Correlation between the mean fragment multiplicity and the multiplicity N_C of charged particles detected in the Miniball/wall for reactions of Au + Au at three bombarding energies E/A = 100, 250, and 400 MeV. The measured quantities are not corrected for the energy and angle dependent detection efficiency of the experimental apparatus (from [39]).

It seems that at intermediate bombarding energies the largest fragment multiplicities are reached in collisions with the largest projectiles at the highest possible energies. However, this no longer holds in the relativistic energy range. The relation between fragment multiplicity and the two parameters, bombarding energy and impact parameter, has been studied by Tsang *et al.* [39]. Using gold beams from SIS at GSI these authors have investigated the reaction ^{197}Au + ^{197}Au at three energies E/A = 100, 250, and 400 MeV. The setup consisted of the MSU Miniball/wall, augmented by the Catania Si-CsI hodoscope and placed in front of the ALADIN spectrometer. Fig. 10 shows the relation between the measured mean IMF multiplicity and the number of charged particles measured with the Miniball/wall. At E/A = 100 MeV a maximum of about 10 fragments of intermediate mass, in the mean, was detected for central collisions. As the bombarding energy is raised, however, the fragment multiplicity in central collisions decreases rather rapidly. The enormous energy deposit produces mostly nucleons and lighter complex particles. At the same time the maximum of the fragment production is shifted to larger impact parameters. The behaviour observed at E/A = 400 MeV is already very similar to that observed at 600 MeV and discussed above. It reflects the sensitivity of the fragmentation pro-

cess to the intensity of the heat source which is controlled by the impact parameter. The impact-parameter dependence of multifragment decays in $^{84}Kr + {}^{197}Au$ reactions, measured over a wide range of bombarding energies by Peaslee *et al.* [40], fits well into these systematics. It will be a rewarding task for the coming years to study the evolution of the multi-fragment processes in this energy region near and above 100 MeV per nucleon and to identify the invariant and the changing physical features. The phenomenon of collective radial motion seems to belong to the latter class.

8. Summary

Reactions at relativistic bombarding energies were found to be an appropriate tool to generate highly excited nuclear systems which undergo multifragmentation as they decay. The observed properties of the spectator decay are the same in peripheral collisions between heavy nuclei and in more central reactions between the heavy and a lighter nucleus, as *e.g.* $^{12}C + {}^{197}Au$ at 600 MeV per nucleon. With even lighter projectiles on heavy targets, according to the systematics, higher bombarding energies will be needed in order to initiate similar decay processes with large probability.

The partition space explored in multifragment decays is well described by the statistical multifragmentation models. The excitation energies obtained from fitting the measured charge correlations are in agreement with those calculated with the BUU model for the input stage in the region of rising fragment multiplicities, *i.e.* up to about 8 MeV per nucleon of excitation energy. The analysis of the fragment energies in the center-of-mass frame of the decaying system yields consistent results. For the more violent collisions the excitation energies needed as input to the statistical models saturate. Here a detailed understanding of the time scales governing the equilibration and decay processes seems indispensable.

The breakup out of an expanded state is confirmed by the analysis of the measured fragment energies in their common rest frame. In the peripheral reactions, the expansion is mainly driven by the thermal pressure. A collective radial flow, if present at all, seems limited to the order of 1 MeV per nucleon. This is in contrast to the large flow values observed for central collisions of heavy symmetric systems.

The observed Z_{bound} scaling is consistent with equilibration as assumed in the statistical multifragmentation models. The charge correlations which all show this scaling feature are reproduced by a variety of conceptually very different models. Some of them are of purely mathematical nature and exhibit critical phenomena for large system sizes.

REFERENCES

[1] J. Bondorf *et al.*, *Nucl. Phys.* **A443**, 321 (1985).
[2] D.H.E. Gross, *Rep. Prog. Phys.* **53**, 605 (1990), and references given therein.
[3] D.H.E. Gross, K. Sneppen, preprint HMI 1993/P1-Gros4
[4] D.H.E. Gross *et al.*, *Phys. Rev. Lett.* **56**, 1544 (1986).
[5] X. Campi, *J. Phys. A* **19**, L917 (1986).
[6] C.J. Pethick, D.G. Ravenhall, *Nucl. Phys.* **A471**, 19c (1987).
[7] G. Bertsch, P.J. Siemens, *Phys. Lett.* **126B**, 9 (1983).
[8] W. Reisdorf *et al.*, contribution to this volume.
[9] A.I. Warwick *et al.*, *Phys. Rev.* **C27**, 1083 (1983).
[10] V. Lips *et al.*, Proceedings of XXXI International Winter Meeting on Nuclear Physics, Bormio 1993, ed. I. Iori, p. 32.
[11] J. Nemeth *et al.*, *Z. Phys.* **A325**, 347 (1986).
[12] J.-J. Gaimard, K.-H. Schmidt, *Nucl. Phys.* **A531**, 709 (1991), and references therein.
[13] E.M. Friedlander, H.H. Heckman, *Treatise on Heavy-Ion Science*, ed. D.A. Bromley, Plenum Press, New York 1985, Vol. 4, p. 403.
[14] see, *e.g.*, Fig. 5 of Ref. [13].
[15] J. Dreute *et al.*, *Phys. Rev.* **C44**, 1057 (1991); *Nucl. Phys.* **A538**, 411c (1992).
[16] P.L. Jain, G. Singh, *Phys. Rev.* **C46**, R10 (1992).
[17] J. Hubele *et al.*, *Z. Phys.* **A340**, 263 (1991).
[18] J. Gosset *et al.*, *Phys. Rev.* **C16**, 629 (1977).
[19] C.A. Ogilvie *et al.*, *Nucl. Phys.* **A553**, 271c (1993).
[20] C.A. Ogilvie *et al.*, *Phys. Rev. Lett.* **67**, 1214 (1991).
[21] P. Kreutz *et al.*, *Nucl. Phys.* **A556**, 672 (1993).
[22] J. Aichelin *et al.*, *Phys. Rev.* **C30**, 107 (1984).
[23] L.G. Sobotka, L.G. Moretto, *Phys. Rev.* **C31**, 668 (1985).
[24] J. Hubele *et al.*, *Phys. Rev.* **C46**, R1577 (1992).
[25] A.S. Botvina, I.N. Mishustin, *Phys. Lett.* **B294**, 23 (1992).
[26] Bao-An Li *et al.*, *Phys. Lett.* **B303**, 225 (1993).
[27] H.W. Barz *et al.*, Report NBI-92-88 (1992).
[28] W.A. Friedman, *Phys. Rev.* **C42**, 667 (1990).
[29] J.B. Garcia, C. Cerruti, Proceedings of XXXI International Winter Meeting on Nuclear Physics, Bormio 1993, ed. I. Iori, p. 144.
[30] R. Botet, M. Ploszajczak, *Phys. Lett.* **B312**, 30 (1993).
[31] S. Leray, S. Souza, Contribution to Second European Biennial Workshop on Nuclear Physics, Megève 1993, preprint LNS/Ph/93-16.
[32] V. Lindenstruth *et al.*, preprint GSI-93-54; V. Lindenstruth, PhD thesis, Universität Frankfurt, 1993, report GSI-93-18
[33] R. Trockel *et al.*, *Phys. Rev. Lett.* **59**, 2844 (1987).
[34] Y.D. Kim *et al.*, *Phys. Rev.* **C45**, 338 (1992).
[35] R. Trockel *et al.*, *Phys. Rev.* **C39**, 729 (1989).
[36] R.T. de Souza *et al.*, *Phys. Lett.* **B268**, 6 (1991).
[37] D.R. Bowman *et al.*, *Phys. Rev. Lett.* **67**, 1527 (1991).

[38] E. Piasecki *et al.*, *Phys. Rev. Lett.* **66**, 1291 (1991).
[39] M.B. Tsang *et al.*, *Phys. Rev. Lett.* **71**, 1502 (1993).
[40] G.F. Peaslee *et al.*, Proceedings of XXXI International Winter Meeting on Nuclear Physics, Bormio 1993, ed. I. Iori, p. 1.